Numerical modelling of hydraulic decompression due to the excavation of tunnel and drifts at the Tournemire underground laboratory

CLAUDE MÜGLER[1], ALAIN GENTY[2] and JUSTO CABRERA[2]
[1]*Commissariat à l'Énergie Atomique, Saclay, 91191 Gif sur Yvette Cedex, France*
[2]*Institut de Radioprotection et de Sûreté Nucléaire, BP 17, 92262*
Fontenay-aux-Roses Cedex, France

Abstract. The Tournemire underground laboratory is situated in a clay formation and consists of a disaffected railway tunnel and two perpendicular drifts. The paper presents modelling and 3D simulations of the hydraulic behaviour of the argillaceous formation around the works. Experimental measurements of porosity, permeability and specific storage coefficients allowed us to model the hydraulic properties of the shale. Numerical simulations are performed with the code CASTEM. Numerical results of hydraulic heads are compared to experimental measurements. Calculations show that the excavation of the tunnel and drifts has induced an hydraulic decompression of the indurated argillaceous formations. The zones of decompression are centred around the structures and extend depending on the values of hydraulic parameters such as permeability and specific storage selected in the model. Six years after the excavation of the drifts, the hydraulic steady state in the fractured zone is not yet reached.

Key words. experimental measurement, hydraulic decompression, numerical simulation, rock permeability, specific storage

1. Introduction

Disposal in deep geological formations is a potential solution for the management of high level radioactive wastes. In these geological disposal concepts, properties of the geological medium are of primary importance. The geological medium is a barrier where radioactive elements are transported by water from the waste to the biosphere. A combination of low water velocity (originating from low hydraulic head gradients and very low rock permeability) and very thick host rock (some hundreds of meters) must therefore be found for the potential host rock so that radionuclides transfer time through the host rock should exceed several times the radionuclides half-lives. In this context, different types of rocks such as granite, salt, volcanic tuff and argillite are extensively studied. Argillaceous formations are of particular interest because their very low permeability and their strong capacity for radionuclide retention give them good confining properties (Lalieux et al., 1996). However, potential strong perturbations of these confining properties can be induced by the boring of the

geological disposal. One of these relevant disturbances is hydraulic decompression. Disturbances can generate higher hydraulic conductivities due to hydro-mechanical processes and modify the velocity fields. Then, the host rock would lost its capacities of delaying radionuclides transfer to the biosphere. Since 1987, the French Institute for Nuclear Radioprotection and Safety (Institut de Radioprotection et de Sûreté Nucléaire, IRSN) attempted to address this issue among others, by developing an experimental research program focusing on the characterization of confinement properties of an argillite and on their potential modifications associated to the disturbances originating from the construction of a geological waste disposal (Barbreau et al., 1994; Boisson et al., 1998; Cabrera et al., 2001; Boisson et al., 2001). This underground laboratory site is located near Tournemire (Aveyron, France) in a Toarcian argillaceous formation. The objective of the paper is to understand and predict the modifications of the hydraulic behaviour in the argillite host rock after the disturbances associated to the possible construction of disposals in such a rock. Modelling of the hydraulic decompression due to the excavation of the works of the laboratory are specifically studied in this paper. Numerical simulations are performed using the data of the Tournemire underground laboratory. First, Section 2 gives a description of the characteristics of the Tournemire site and a description of the geometry of the works. Section 3 gives a description of the model and numerical methods used to perform the simulations. In Section 4, a detailed study of the numerical results is presented and discussed and, finally, experimental and numerical results are compared.

2. Description of the Tournemire underground laboratory

2.1. GEOLOGICAL DESCRIPTION

The Tournemire site is located in the South of France (Aveyron) and is characterized by a sub-horizontal indurated argillaceous layer located between two limestone aquifers. This site was selected because of its geological simplicity. A disaffected old railway tunnel provides direct access to the argillaceous formation. The location and a geological vertical cross section of the site are shown in Figure 1. The geology of the Tournemire site can be modeled by three simplified sedimentary layers. All these layers belong to the early and middle Jurassic period:

- the lower layer is an aquifer made up of about 300 m of limestone and dolomite of the Hettangian, Sinemurian and Carixian series;
- the middle layer is made up of about 250 m of marl and argillite of the Domerian, Toarcian and lower Aalenian series;
- the upper layer is another aquifer made up of about 250 m of limestone and dolomite of the upper Aalenian, Bajocian and Bathonian series.

All the geological layers lean over to the North (inclination of $-4°$). On the other hand, the inclination of the tunnel is equal to $+0.83°$ to the North. The tunnel
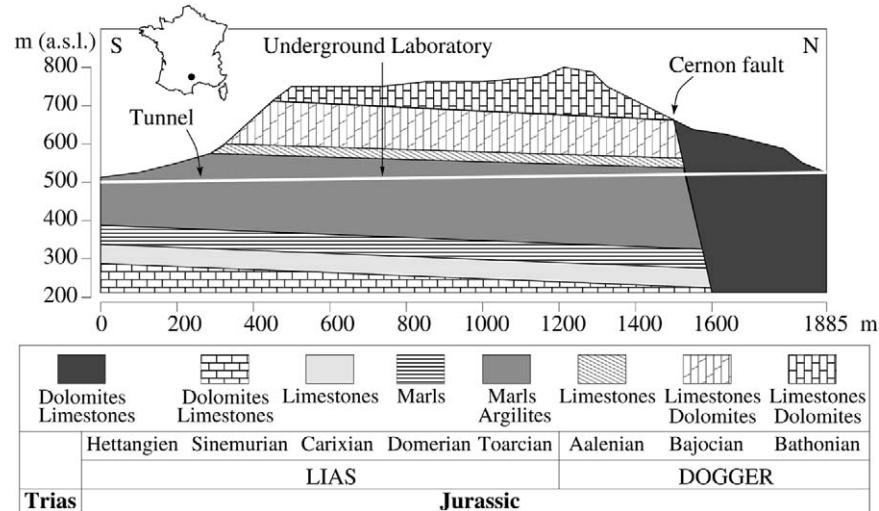
Figure 1 Geological vertical cross section of the Tournemire site

crosses the Toarcian claystone of the middle layer. In the three layer model presented above, the fluid flow essentially occurs in the upper and lower layers made up of limestone and dolomite. These layers are more easily broken and consequently more fractured. However, the characterization of the experimental site has revealed the presence of fractures of tectonic origin in the argillaceous formations. The fracturing is mainly sub-vertical and includes microfissures (millimeter scale), fractures (centimeter scale) sealed by calcite and faults (decimeter to meter scale). Most of this fracturing is associated to the North/South trending Pyrenean compression event (40–50 million years ago). The characterization of the experimental site has revealed the presence of two vertical blocks in the argillaceous formation: a densely fractured west block and a sparsely fractured east block (see Figure 2). A vertical fault, oriented along a North/South to North-West/South-East axis, divides the two blocks.

2.2. GEOMETRY OF THE TUNNEL AND DRIFTS

The underground laboratory is located in an old disaffected railway tunnel bored in 1888. This tunnel is 1885 m long, 4.66 m width and 5.63 m high. In 1996, two 30 m long drifts were drilled perpendicularly to the tunnel. A sketch of the vertical sections of the tunnel and drifts is given in Figure 3 and an overall view of the works is given in Figure 4. The entrance and the exit of the tunnel are at an altitude of 506.88 m and 534.19 m, respectively.

2.3. FEATURES OF THE ARGILLACEOUS FORMATIONS

The argillaceous media corresponds to well-compacted argillites and marls due to lithostatic pressure and diagenetic processes. Boreholes have been used to obtain
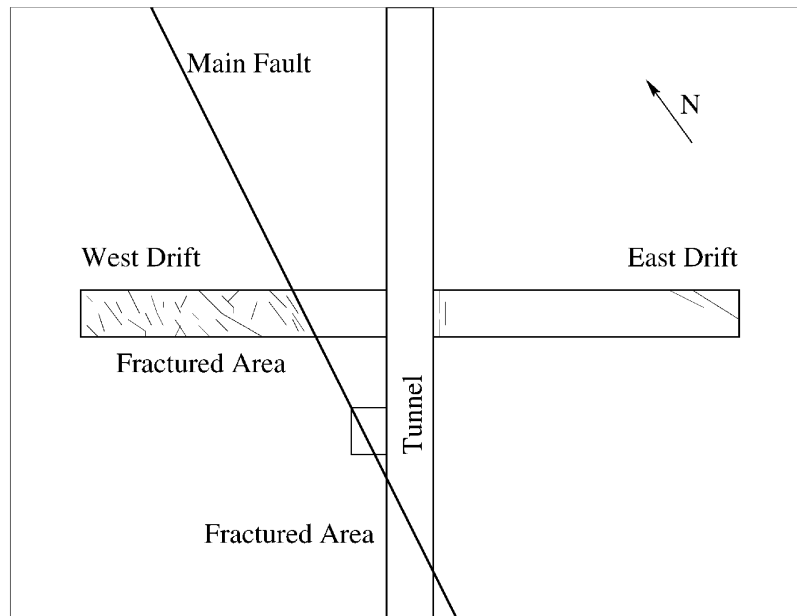
Figure 2   Structural and tectonic sketches around the tunnel and the drifts of the Tournemire site

geological, stratigraphic, tectonic and hydrogeological characteristics of the clay formation surrounding the tunnel (Boisson et al., 1998; Cabrera et al., 2001).

Porosity

The indurated argillite of the site of Tournemire is a very low porous material. Its porosity ω is lower than 10% and the mean pore diameter is less than 20 Å. Both
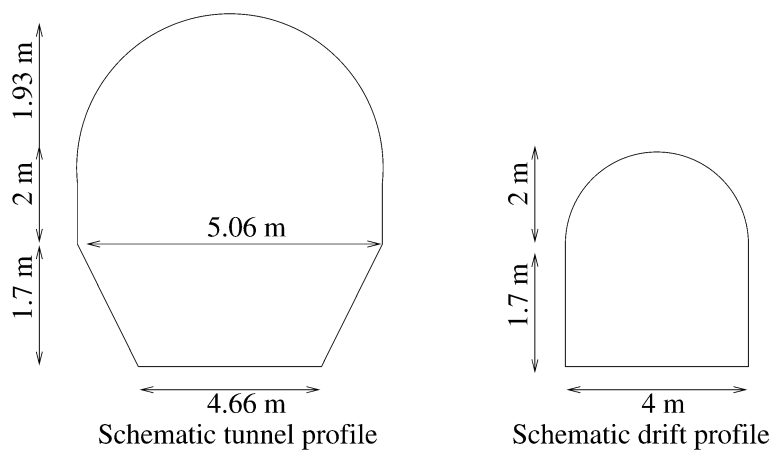

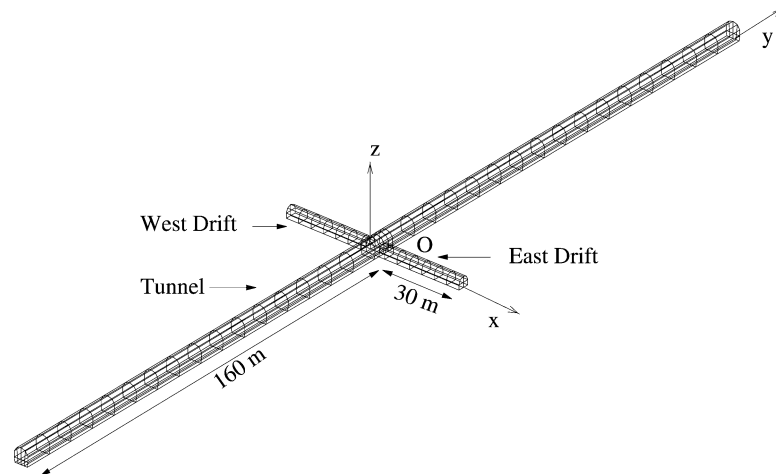Figure 3   Sketches of the vertical sections of the tunnel and drifts

Figure 4   Overall view of the tunnel and drifts

of them slightly decrease with depth. As a consequence, measurements of the poros-
ity value by means of usual experimental methods such as mercury porosimetry is
very difficult. Furthermore, the effective porosity of the argillite is quite different
from its total porosity because of the presence of a considerable quantity of adsorbed
water. According to the measurements, the effective porosity varies between 5% and
8% although the total porosity is about 9%. In this model, an intermediate value of
$\omega = 6\%$ is considered.

Permeability

Measurements of permeability have been performed in-situ but also on various core
samples of argillite (Boisson et al., 1998) with the pulse-test technique (Hsieh et al.,
1981; Neuzil et al., 1981). The obtained values are very low and strongly depend
on the measurement conditions. Figure 5 clearly shows the dispersion of the values.
Permeabilities obtained on cores are the lowest ones and lie between 10^{-13} and
$10^{-15}\,\mathrm{ms^{-1}}$. Those particularly small values have already been pointed out for similar
argillites (Neuzil, 1994; Thury et al., 1999). They seem to correspond to the perme-
ability of the argillite matrix. On the other hand, in-situ permeability measurements
take into account the possible presence of more permeable fractured zones around
the boreholes. The obtained values are consequently higher and lie between 10^{-11}
and $10^{-13}\,\mathrm{ms^{-1}}$. In Figure 5, permeability values are very high in the Aalenian and
Carixian series because these sedimentary layers are aquifers made of limestone
and dolomite.
   Measurements of permeability and specific storage coefficients in this study
allowed to model the hydraulic properties of the shale in the argillaceous formation.
In the model, in order to take into account the presence of tectonic fractures, two
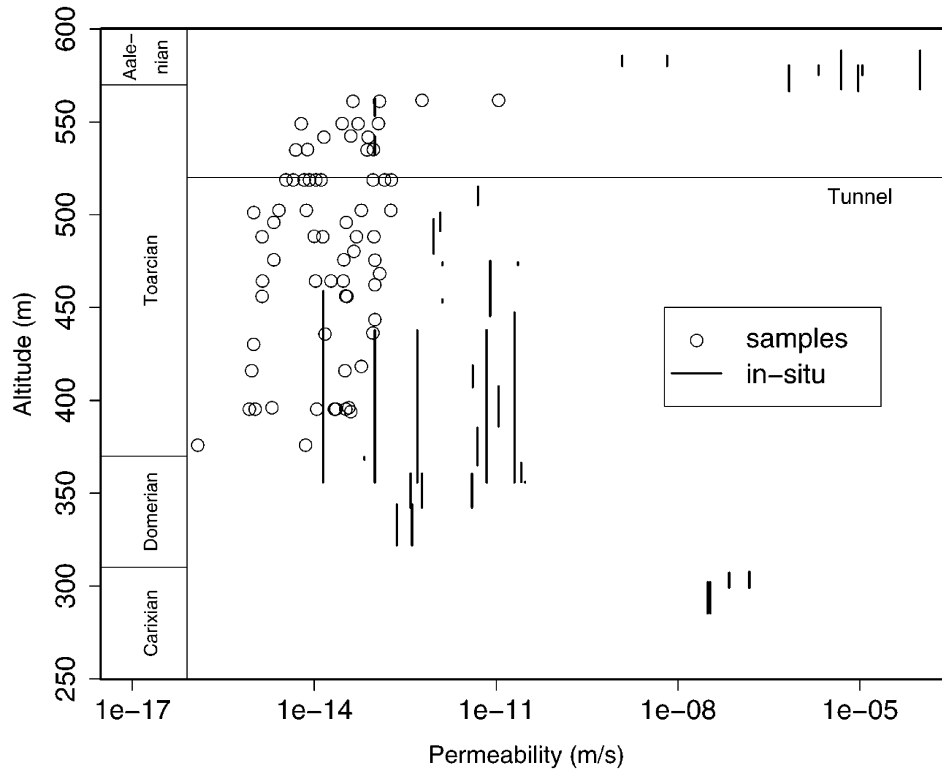
Figure 5   Variation of measured permeability with altitude

zones were modelled, the fractured one having a permeability two orders of magnitude greater than the unfractured one. Although the faults are deeply rooted (certainly until the lower aquifer), their influence on the permeability is only important in the upper Toarcian geological layer where the permeability in the unfractured zone is particularly low. According to the experimental measurements, the following permeability coefficients were chosen:

- unfractured upper Toarcian: $K = 10^{-14}\,\mathrm{m\,s^{-1}}$;
- fractured upper Toarcian: $K = 10^{-12}\,\mathrm{m\,s^{-1}}$;
- medium and lower Toarcian: $K = 10^{-11}\,\mathrm{m\,s^{-1}}$;
- domerian: $K = 2 \times 10^{-13}\,\mathrm{m\,s^{-1}}$.

Specific storage coefficient

The specific storage coefficient S_s ($\mathrm{m^{-1}}$) of an aquifer is given by (de Marsily, 1994)

$$S_s = \rho \omega g \left(\beta_l - \beta_s + \frac{\alpha}{\omega} \right), \tag{1}$$

where,

- ρ is the mass per unit volume of fluid (for water, $\rho = 10^3 \, \mathrm{kg \, m^{-3}}$);
- ω is the porosity;
- g is the acceleration due to gravity ($g = 9.81 \, \mathrm{m \, s^{-2}}$);
- β_l is the compressibility coefficient of the liquid. For water, $\beta_l = 5 \times 10^{-10} \, \mathrm{m \, s^2 \, kg^{-1}}$;
- β_s is the compressibility coefficient of the solid grains. In practice, β_s is often neglected because for most minerals $\beta_s \simeq \beta_l/25$;
- α is the compressibility coefficient of the soil ($\mathrm{m \, s^2 \, kg^{-1}}$).

In the case of an isotropic medium, the mechanical properties are defined by only two coefficients, Young's modulus E ($\mathrm{kg \, m^{-1} s^{-2}}$) and Poisson's ratio v. The compressibility coefficient of the soil α is then given by (de Marsily, 1994)

$$\alpha = \frac{3(1 - 2v)}{E}. \tag{2}$$

Compressibility tests have shown that the Tournemire shale behaviour is transversely isotropic: the main anisotropic direction is perpendicular to bedding planes and the shale behaviour in the bedding planes is quite isotropic (Niandou, 1997). The Young's modulus in the direction normal to the bedding planes (z-axis) is noted E_z and the Young's modulus in any direction in the bedding planes (x-axis and y-axis) which represent the isotropic plane of the shale is noted E_x. The coefficient v_{ij} (v_{xy}, v_{zx} or v_{xz}) is the Poisson's ratio defining the lengthening deformation along the direction i due to the normal stress in the direction j. An equivalent Young's modulus E and Poisson's ratio v can be calculated (Thouvenin, 1999) as:

$$E = \frac{v_{zx}^2 E_z + (2v_{xy} + 1)E_x}{(1 + v_{xy})^2} \quad \text{and} \quad v = \frac{v_{zx}^2 E_z + v_{xy} E_x}{E_x(1 + v_{xy})}. \tag{3}$$

Analysis of the elastic behaviour of the Tournemire shale in laboratory have shown that the Young's moduli E_z and E_x increase with the mean stress (Niandou, 1997). However, in-situ measurements (Rejeb, 1999) have given the following mean values

$$E_x = 27680 \pm 4040 \, \mathrm{MPa} \quad \text{and} \quad v_{xy} = 0.17 \pm 0.03$$
$$E_z = 9270 \pm 490 \, \mathrm{MPa} \quad \text{and} \quad v_{zx} = 0.2 \pm 0.03$$

And finally, Eq. (3) yields $E = 27400 \, \mathrm{MPa}$ and $v = 0.16$. With such values, the specific storage coefficient S_s given by Eq. (1) is equal to $10^{-6} \, \mathrm{m^{-1}}$.

The experimental determination of the specific storage coefficient S_s is quite difficult. However, in-situ measurements showed that this coefficient is quite independent of the geological layer and always lies between 3×10^{-7} and $9 \times 10^{-7} \, \mathrm{m^{-1}}$ (Boisson et al., 1998). Experimental measurements of S_s which have been performed in the Callovo-Oxfordian claystone of the Paris basin give quite identical values: S_s lies between 10^{-7} and $3 \times 10^{-6} \, \mathrm{m^{-1}}$ (Cosenza et al., 2002). As can be seen for the Tournemire site,

the calculated value of S_s and the measured one are of the same order of magnitude although several simplifications have been performed in the calculation. Finally, for the simulations, an intermediate experimental value of $S_s = 5 \times 10^{-7}\,\mathrm{m^{-1}}$ is used.

2.4. IN-SITU HYDRAULIC-HEAD EVALUATION

Hydraulic-head measurements have been performed in the lower and upper aquifers. Experimental results are in good agreement with hydrogeological observations issued from springs, draining lines, etc. (Barbreau et al., 1994). The hydraulic head is approximately equal to 590 and 460 m in the upper and the lower aquifer, respectively. Hydraulic heads are expressed in relation to the mean sea level in the same way as topographic elevations. A map of the hydraulic-head field in the lower aquifer is deduced from in-situ regional measurements. This is not the case of the upper aquifer where only one measure of the hydraulic head has been done.

In the indurated clay formation, hydraulic-head measurements are more difficult because of the very-low permeability of the argillite. After a perturbation induced by drilling operations, it needs a very long time to reach the steady-state. As a consequence, experimental results are not always accurate. They are given in Figure 12 where they are compared to numerical results (see Section 4.4).

3. Numerical model

In the model, we assume that the fluid movement in the argillaceous formation is only of the darcean type. The hydraulic-head evolution is then modelled by the diffusion equation in use for confined aquifer (de Marsily, 1994) and given by

$$S_s \frac{\partial}{\partial t} h - \mathrm{div}\,\overline{\overline{K}}\,\vec{\nabla} h = 0, \tag{4}$$

where h is the hydraulic head (m), $\overline{\overline{K}}$ is the permeability tensor ($\mathrm{ms^{-1}}$) and S_s is the specific storage coefficient ($\mathrm{m^{-1}}$). The fracture network is modelled by an equivalent porous media as well as the unfractured zone. Values of the permeability in the fractured and unfractured zones differ by two orders of magnitude.

In the steady state, Eq. (4) reduces to

$$\mathrm{div}\,\overline{\overline{K}}\,\vec{\nabla} h = 0, \tag{5}$$

and, according to the Darcy law given by

$$\vec{U} = -\overline{\overline{K}}\,\vec{\nabla} h, \tag{6}$$

where $\vec{U}$ is the Darcy velocity ($\mathrm{ms^{-1}}$), Eq. (5) becomes

$$\begin{cases} \mathrm{div}\,\vec{U} = 0 \\ \vec{U} \quad = -\overline{\overline{K}}\,\vec{\nabla} h \end{cases} \tag{7}$$

3.1. NUMERICAL SCHEME

Numerical simulations were performed with the code CASTEM (C.E.A, 2000; Dabbene, 1998) that uses a mixed-hybrid finite element method to solve the diffusion equation. In a classical finite element method, the diffusion equation given by Eq. (4) or by Eq. (7) is solved only for the hydraulic head. Once the charge has been evaluated, the Darcy velocity is then calculated according to Eq. (6). On the other hand, in a mixed finite element method, the diffusion equation is simultaneously solved for the hydraulic head and for the velocity. The advantage of this method is to ensure simultaneously the mass conservation and the flux continuity. This method is particularly well suited to the resolution of hydrogeological problems where flow properties such as permeability can vary within several orders of magnitude (Chavent et al., 1991). In the mixed-hybrid formulation, the system of equations is solved using a new variable called the trace of the head and which corresponds to the value of the hydraulic head on the edges of each cell. The hydraulic head and the velocity at the center of the cells are then deduced from the values of the trace of the head. In case only the steady state is required, calculations will consist in solving the Darcy equation given by Eq. (7). On the other hand, if the transient regime is required, the complete diffusion equation given by Eq. (4) must be solved.

Modelling and numerical simulations of hydraulic decompression due to the excavation of tunnel and drifts at the Tournemire underground laboratory have been performed according to the following steps:

- In a first step, the hydraulic regime of the unperturbed site, i.e. before the excavation of the tunnel and the drifts is calculated. This steady state is obtained by solving Eq. (7) in all the domain.
- In a second step, the hydraulic regime obtained after the excavation of the tunnel alone is estimated. As the tunnel was bored in 1888, it can be assumed that the steady state is reached. Therefore, only the Darcy equation given by Eq. (7) is solved.
- In a third step, the purpose is to quantify the effects of the excavation of the two drifts. As the drifts were bored in 1996, the transient state given by Eq. (4) is to be solved. In this case, the initial fields for the hydraulic head and the velocity correspond to the results obtained from the previous calculations in step 2.

3.2. MESH DESCRIPTION

The purpose of the calculations is to quantify the impact of the presence of the works on the hydraulic regime in the surrounding argillaceous formation. Consequently, the size of the simulated region must include the two drifts and a long enough part of the tunnel. The domain extension must be sufficient to avoid influences due to the boundary conditions. The lower and upper boundary conditions are respectively the lower and upper limestone aquifers. The domain extension along the tunnel is chosen equal

to 320 m to take into account the zones where the hydraulic head has been measured in boreholes. Along the drifts direction (perpendicular to the tunnel direction), the domain extension is chosen equal to five times the drift length, i.e. equal to 300 m. Indeed, analytical solutions of the problem of the disturbance of steady hydraulic head field in uniform medium by an object of different permeability buried in it show that the perturbation rapidly decreases with the distance r to the center of the object. It varies as $(a/r)^3$ for a spherical object of radius a and as $(a/r)^2$ for a cylindrical one (Carslaw et al., 1959). Finally, the size of the simulated region is $300 \times 320 \times 260.7 \, m^3$. The mesh is refined in the upper Toarcian geological layer near the structures in order to accurately simulate the decompression. The lowest zone size is equal to $2 \times 2 \times 2 \, m^3$. Calculations with various grids have shown that spatial convergence is reached. On the other hand, the mesh far from the structures is coarse. The largest zone size is equal to $10 \times 10 \times 30 \, m^3$. The entire 3D mesh is done of 34 760 cells (see Figure 6). As specified in Figure 4, the x-axis and y-axis are in the horizontal plane which includes the work floor and correspond to the main direction of the east drift and of the tunnel, respectively. The z-axis indicates the vertical direction. The origin of the coordinates system is located in the work floor at the intersection of the tunnel and the drifts.
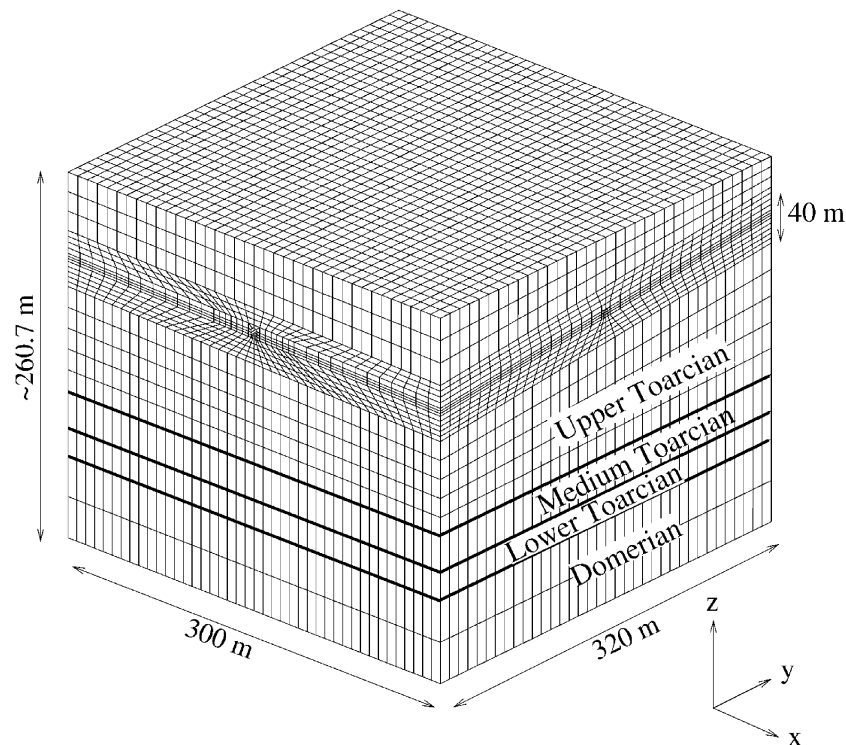

Figure 6   Entire 3D mesh generation of 34 760 cells

3.3. INITIAL AND BOUNDARY CONDITIONS

Figure 7 gives a 3D map of the permeability coefficients used to simulate the various geological layers, as mentioned in Section 2.3.

Fixed hydraulic heads are imposed at the top and bottom of the argillaceous formation, in agreement with the measurements in the upper and lower aquifers (see Section 2.4). The open structures are always at atmospheric pressure. As this pressure is the reference pressure, the hydraulic head at the excavated structures/rock formation interface is constant and equal to the altitude, i.e. 510 m. The other boundary conditions are of no-flux type.

4. Numerical results

In this section, the results of the 3D numerical simulations of the Tournemire site are presented. All these calculations use the same mesh around the works. However, according to the situation, the mesh includes or does not include the volumes which correspond to the works.

4.1. SIMULATION OF THE UNPERTURBED SITE

The purpose of this preliminary simulation is to calibrate the hydraulic-head field of the unperturbed site, previous to any excavation. So, the tunnel and the drifts
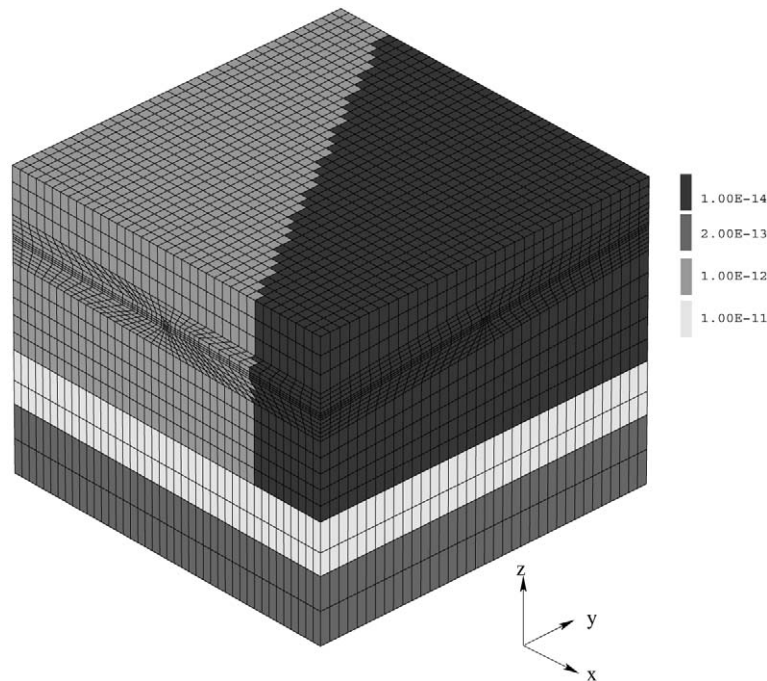

Figure 7   Permeability coefficients in the geological layers (ms^{-1})

are not yet excavated and the Darcy equation given by Eq. (7) is solved in all the domain.

Figures 8(a)–(d) show the hydraulic-head distributions in all the domain including some cross sections. Figure 8(b) gives an upper view of the cross section in the horizontal plane $z = 0$. The North and the South are respectively at the top and the bottom of this figure. This figure shows the slight increase of the head pressure from the South to the North, due to the inclination of the geologic layers. The vertical cross sections given in Figures 8(c) and (d) show the influence of the west fractured zone which is more permeable than the east unfractured zone. The hydraulic head at the level of the tunnel is equal to 570 m.
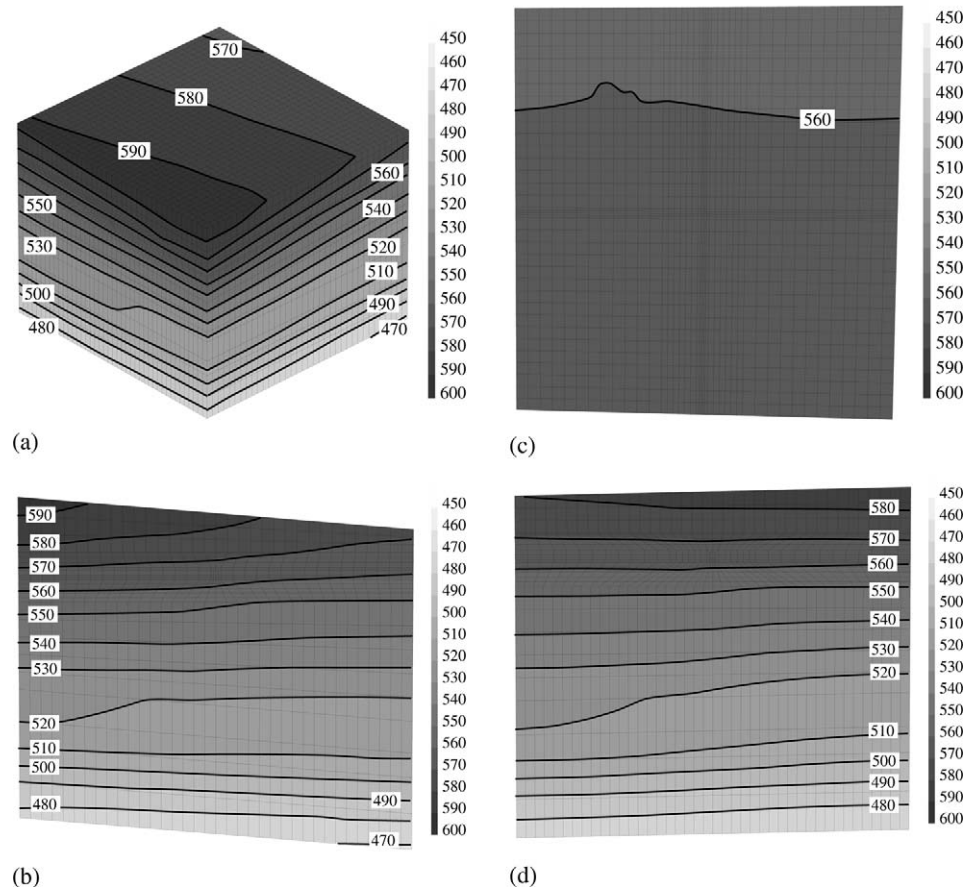

(a)

(c)

(b)

(d)

Figure 8   Hydraulic head in the unperturbed site: (a) in all the domain; (b) in the horizontal plane $z = 0$ (plane which includes the work floor); (c) in the vertical plane $x = 0$ (plane which includes the axis of symmetry of the tunnel); (d) in the vertical plane $y = 0$ (plane which includes the axis of symmetry of the drifts)

4.2. SIMULATION AFTER THE EXCAVATION OF THE TUNNEL

The purpose of this second model is to quantify the hydraulic decompression due to the excavation of the tunnel alone. As already said, assuming the steady state to be reached, the Darcy equation given by Eq. (7) is solved in the domain around the excavated tunnel.

Figures 9(a)–(d) show the hydraulic-head distributions in all the domain including some cross sections. Comparing Figures 8 and 9 clearly show the hydraulic decompression due to the excavation of the tunnel. The hydraulic-head decrease extends on several tens of meters around the tunnel.
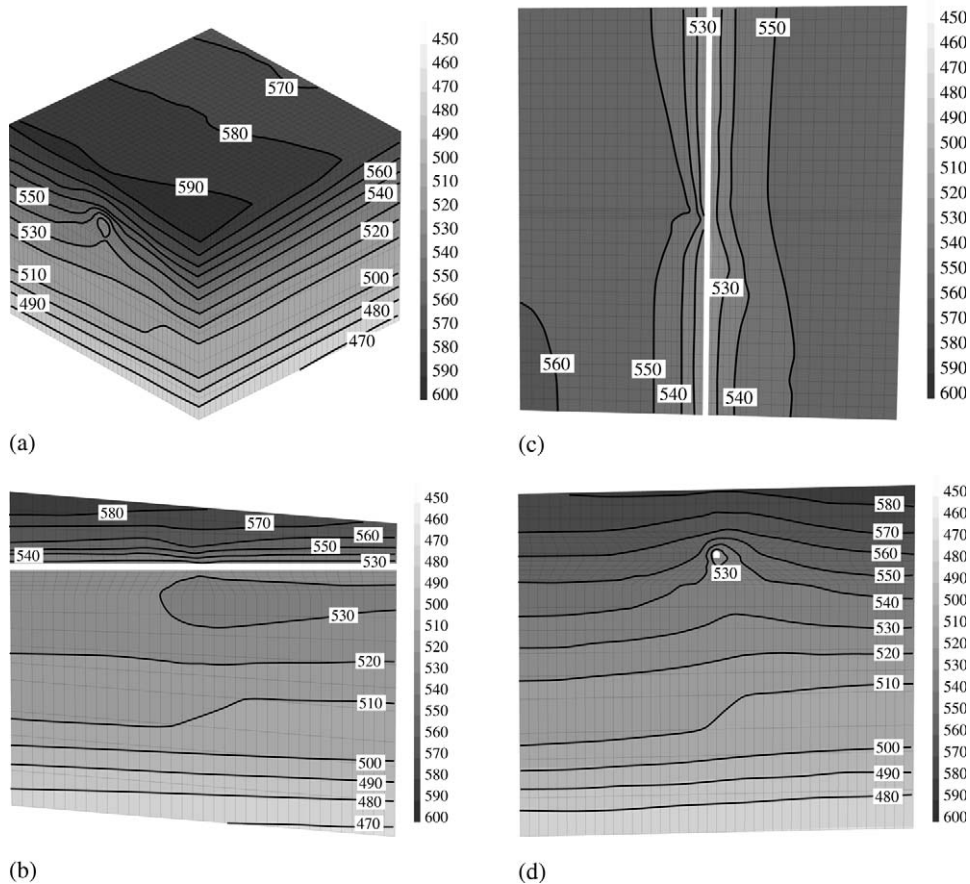

Figure 9   Hydraulic head in the site after excavation of the tunnel: (a) in all the domain; (b) in the horizontal plane $z = 0$ (plane which includes the work floor); (c) in the vertical plane $x = 0$ (plane which includes the axis of symmetry of the tunnel); (d) in the vertical plane $y = 0$ (plane which includes the axis of symmetry of the drifts)

4.3. SIMULATION AFTER TUNNEL AND DRIFTS EXCAVATION

The third and last model simulates the hydraulic behaviour of the site after tunnel and drifts excavation. As already mentioned, assuming the steady state condition has not yet reached, the diffusion equation given by Eq. (4) is solved in the domain around the excavated tunnel and drifts. The initial time is the year 1996 when the drifts were excavated and the excavation is assumed instantaneous. The initial hydraulic field noted $h(x, y, z, t_0)$ corresponds to the steady state obtained after the tunnel excavation.

Figures 10(a)–(f) show the hydraulic-head distributions in some cross sections five years after the excavation of the drifts. The variation of the hydraulic head $h(x, y, z, t_0) - h(x, y, z, t)$ is also presented. These figures clearly show the expansion of the hydraulic-head disruption around the drifts. The disturbed zone is larger in the west fractured zone and increases with time: after five years, the decompression spreads over about five cells, i.e. about 20 meters around the west drift. Around the east drift, the mesh is too coarse to describe precisely the too weak decompression which only spreads over one cell. According to Eq. (4), the disruption length scales as $\sqrt{Dt}$ where $D = K/S_s$ is the hydraulic diffusivity ($\mathrm{m^2 s^{-1}}$). In the fractured zone, $D = 2 \times 10^{-6}\,\mathrm{m^2 s^{-1}}$ and in the unfractured zone, $D = 2 \times 10^{-8}\,\mathrm{m^2 s^{-1}}$. At $t = 5\,years$, this length equals 1.8 and 18 m in the unfractured and fractured zone, respectively. These values are in good agreement with the magnitude of the expansion of the decompression obtained from the numerical simulation (see Figures 10(e) and (f)). It is to be pointed out that the decompression occurs only around and near the drifts. Far from the drifts even near the tunnel (see for example Figure 10(d)), the site is unperturbed.

Figure 11 displays the hydraulic head variation $h(x, y, z, t_0) - h(x, y, z, t)$ versus time at five various locations in the fractured zone at $x = -20\,\mathrm{m}$, $y = 0\,\mathrm{m}$, $z = 0, -5.6, -9.2, -20$ and $-36.9\,\mathrm{m}$, respectively. These curves show that the steady state is not yet reached around the six-years old drift. However, the hydraulic-head variation are nowadays too low to be experimentally measured.

4.4. COMPARISON OF EXPERIMENTS AND SIMULATIONS

Several measurements of the hydraulic head have been performed in-situ in several boreholes, before the drifts excavation (Boisson et al., 1998). Such measurements are very difficult and experimental results are not always accurate. Figure 12 displays the variation of the hydraulic head versus the altitude. In this figure, experimental values are represented with errorbars which are sometimes very large (see for example the ID1 or ID3 boreholes). Numerical hydraulic heads obtained from simulations correspond to the hydraulic-head profile against the vertical axis Oz before (dashed line) and after (solid line) the tunnel excavation. Numerical results and experimental measurements of hydraulic heads are in quite good agreement. Calculations clearly show that the excavation of the tunnel has induced an hydraulic decompression of the indurated argillaceous formations.
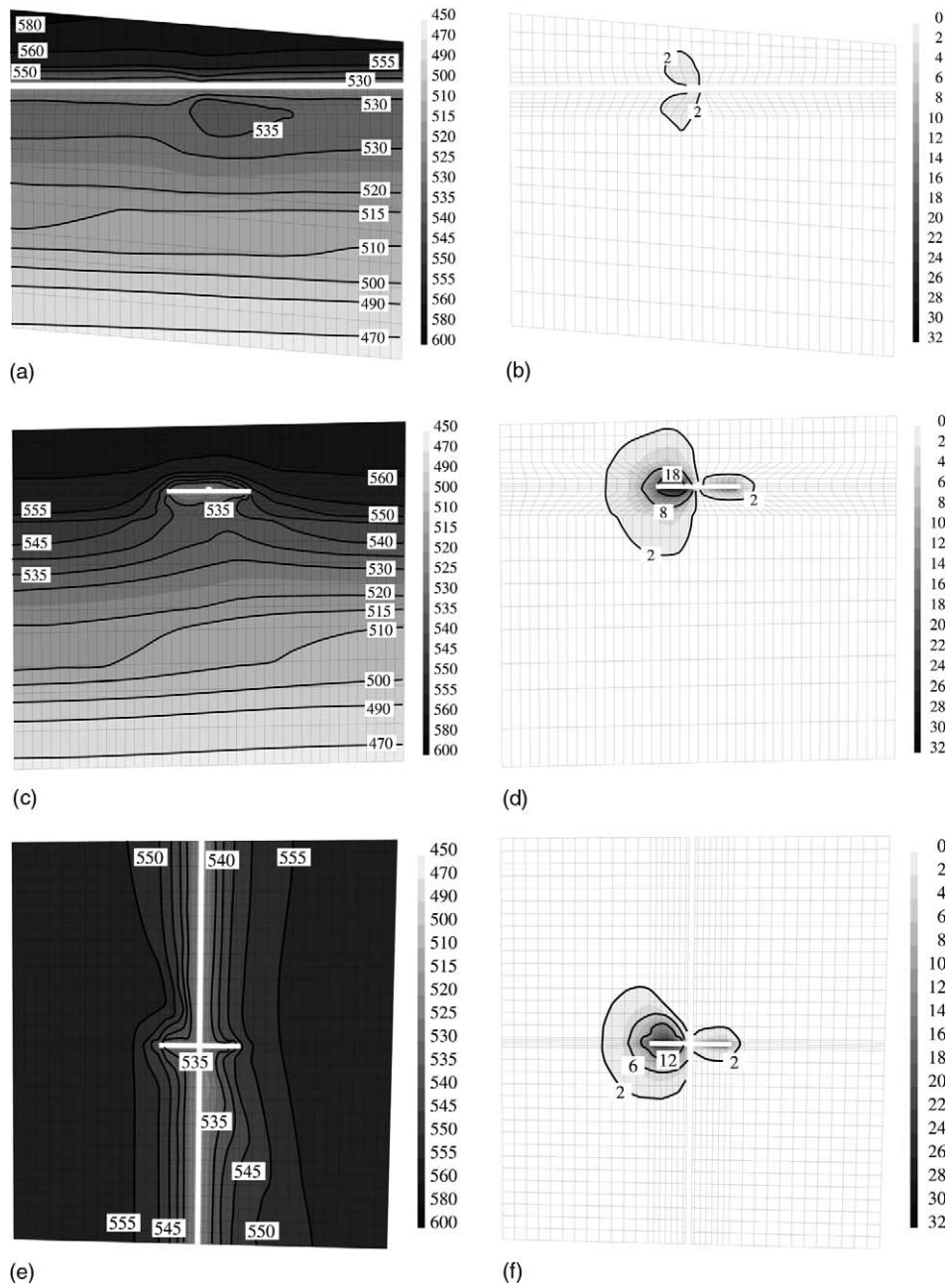
Figure 10   Hydraulic head in the site and variation of the hydraulic head $h(x, y, z, t_0) - h(x, y, z, t)$, after excavation of the tunnel and the drifts. Unsteady state at $t = 5$ years: (a) and (d) in the vertical plane $x = 0$; (b) and (e) in the vertical plane $y = 0$; (c) and (f) in the horizontal plane $z = 0$
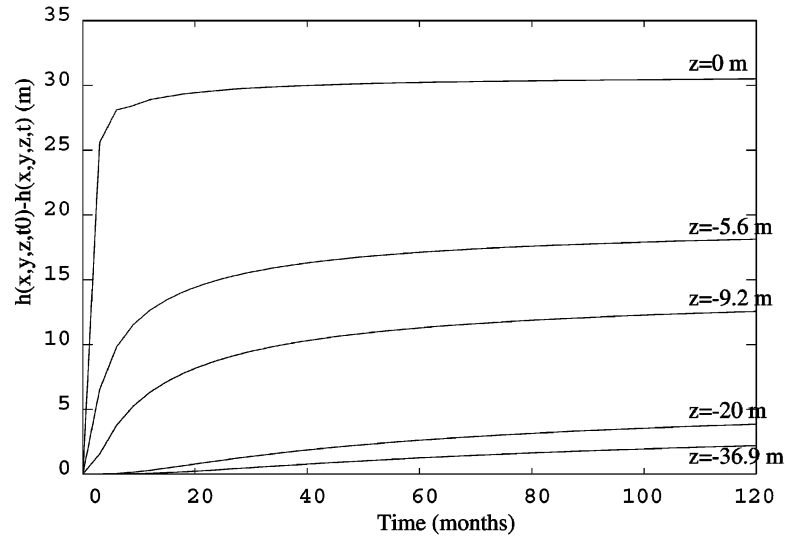
Figure 11   Hydraulic head difference versus time after excavation of the drifts, under the west drift (fractured zone), at $x = -20$ m, $y = 0$ and various z
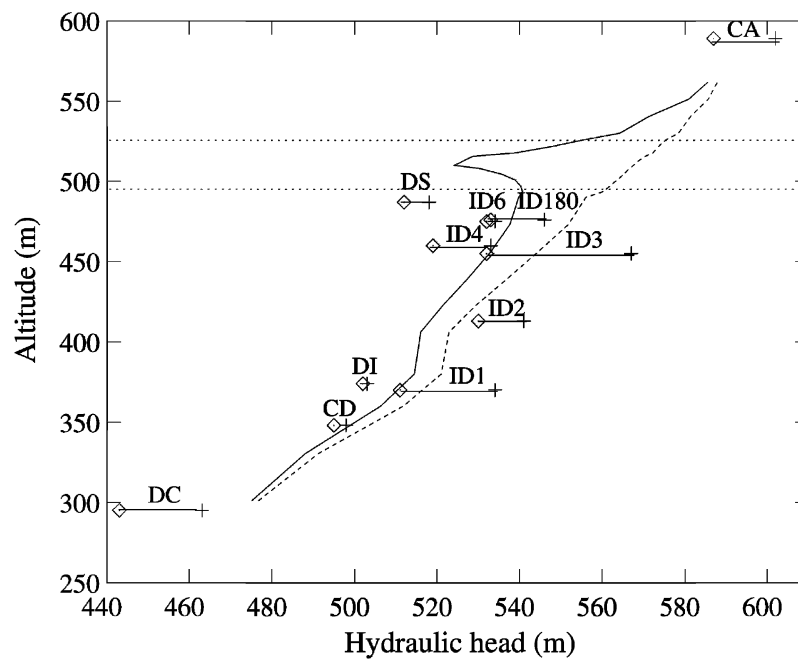

Figure 12   Comparison between the measured and estimated hydraulic heads, after excavation of the tunnel. The dashed and solid lines correspond to the results of the simulations before and after excavation of the tunnel, respectively. Symbols correspond to in-situ measurements
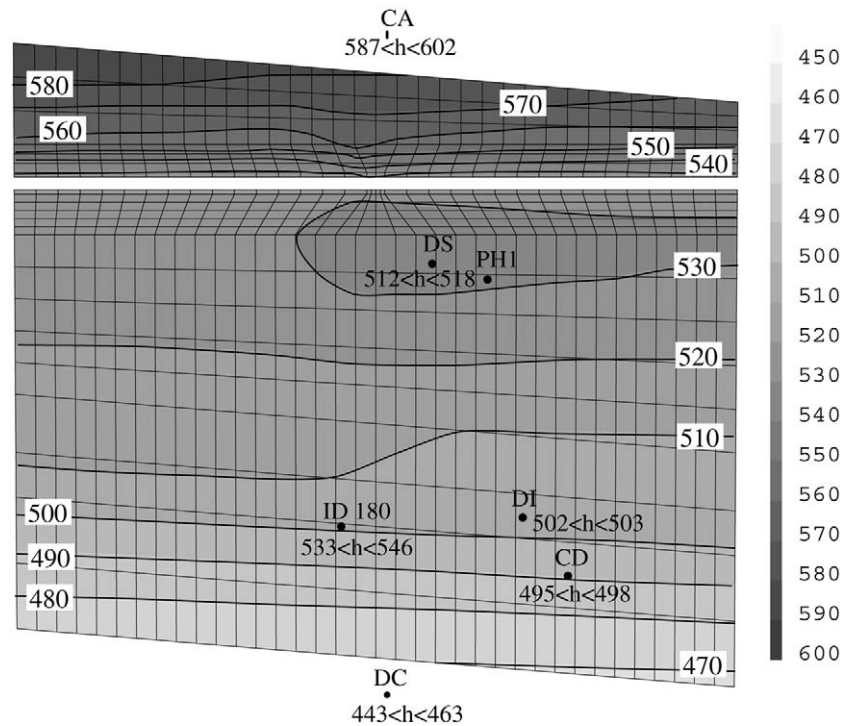
Figure 13   Comparison between the measured and estimated hydraulic heads h in the vertical plane $x = 0$, after excavation of the tunnel

The more affected zone (delimited by two dotted lines in Figure 12) has a vertical extension equal to 35 m, i.e. about 15 m on both sides of the tunnel, which is quite equal to 3 times the tunnel height. Far from the tunnel, the two numerical profiles are not superimposed on one another which are about 5 m apart. This discrepancy may be due to the coarse spatial discretisation. Indeed, in the geological layers far from the works, the zone sizes are very large (about 20 or 30 m). Figure 13 gives the same comparison in another representation which takes into account the position of the point measurement in the boreholes in the clay formation. This figure shows that all boreholes are too deep to allow us to measure the hydraulic decompression due to the works. On the contrary, hydraulic-head measurements just below the west drift would help to validate the hydraulic modelling of the site presented in this paper.

5. Conclusion

The purpose of this paper was to demonstrate our ability to understand and predict with help of numerical simulation the hydraulic decompression behaviour due to theexcavation of tunnel and drifts in a very low permeable rock like Tournemire

argillite. The comparison between numerically estimated heads and in-situ measured ones shows a rather qualitative agreement (with a maximum difference of about ten meters) and achieved our objectives. From a more quantitative point of view, 3D numerical simulations clearly show the zones where the hydraulic decompression is larger. These zones are centred around the structures and extend depends on the values of hydraulic parameters such as permeability and specific storage selected in the model. The hydraulic decompression zone in the clay surrounding the west drift is ten times wider than around the east drift pointing out the effect of two orders of magnitude difference on permeability between the two areas. The choice of the hydraulic parameters to use in the various geologic layers was made on experimental measurements values. However, the porosity and the permeability of the argillaceous formation surrounding the works are very low, measured values are strongly dispersed and experimental methods maybe not very accurate. The rather good agreement between estimated and measured heads validate a posteriori the values used. This study provides insight to plan and conduct further measurements in order to improve knowledge of the hydraulic features of the shale. For example, hydraulic-head measurements in about 10-m deep boreholes in the drift would more precisely validate the model and the permeability values used.

References

Barbreau, A. and Boisson, J.-Y. (1994) Caractérisation d'une formation argileuse. Synthèse des principaux résultats obtenus à partir du tunnel de Tournemire (1991–1993), EC Final Rep EUR 15756, Technol. Series. CEC Nuclear Science, Luxembourg.

Boisson, J.-Y., Cabrera, J. and De Windt, L. (1998) Etude des écoulements dans un massif argileux, laboratoire souterrain de Tournemire, Report CEA-IPSN DPRE/SERGD 98/06, France.

Boisson, J.-Y., Bertrand, L., Heitz, J.-F. and Moreau-Le Golvan, Y. (2001) In-situ and laboratory investigations of fluid flow through an argillaceous formation at different scales of space and time, Tournemire tunnel, Southern France, *Hydrogeology Journal*, **9**, 108–123.

Cabrera, J., Volant, P., Baker C., Pettitt W. and Young, R.P. (1999) *Structural and geophysical investigations of the EDZ in indurated argillaceous media: The tunnel and the galleries of the IPSN Tournemire site, France, in Proceedings of the 37th U.S. Rock Mech. Sympo*. Vail/USA/6–9 June 1999, pp. 957–964.

Cabrera, J., Beaucaire, C., Bruno, G., De Windt, L., Genty, A., Ramambasoa, N., Rejeb, A., Savoye, S. and Volant, P. (2001) Projet Tournemire. Synthèse des programmes de recherche (1995–1999), Report IRSN/DPRE/SERGD 01/19, France.

Carslaw, H.S. and Jaeger, J.C. (1959) *Conduction of heat in solids*, Clarendon Press, Oxford.

C.E.A., CASTEM 2000 User's Manual, english Version, C.E.A.

Chavent, G. and Roberts, J.-E. (1991) A unified physical presentation of mixed, mixed-hybrid finite elements and standard finite difference approximations for the determination of velocities in waterflow problems, *Adv. Water Resources*, **14**(6), 329–348.

Cosenza, Ph., Ghoreychi, M., de Marsily, G., Vasseur, G. and Violette, S. (2002) An integrated approach to predict properties of argillaceous rocks, in Poromechanics II, In: J.-L. Auriault et al. (eds.), *Proceedings of the second Biot conference on poromechanics*, A.A. Balkema Publishers, Grenoble, 157–163.

Dabbene, F. (1998) Mixed-hybrid finite elements for transport of pollutants by underground water, In: *Proceedings of the 10th Int. Conf. on Finite Elements in Fluids*, U.S.A., pp. 456–461.

Hsieh, P.A., Tracy, J.V., Neuzil, C.E. and Silliman, S.E. (1981) A transient laboratory method for determining the hydraulic properties if 'tight' rocks – I: Theory, *Int. J. Rock Mech. Min. Sci. and Geomech. Abstr.*, **18**, 245–252.

de Marsily, G. (1986) *Quantitative Hydrogeology*, Academic Press Inc. (London).

Lalieux, P., Thury, M. and Horsman, S. (1996) Radioactive waste disposal in argillaceous media, *OCDE/NEA Newsletter*, **34**.

Neuzil, C.E., Cooley, C., Silliman, S.E., Bredehoeft, J.D. and Hsieh, P.A. (1981) A transient laboratory method for determining the hydraulic properties if 'tight' rocks – II: Application, *Int. J. Rock Mech. Min. Sci. and Geomech. Abstr.* **18**, 253–258.

Neuzil, C.E. (1994) How permeable are clays and shales? *Water Resources Research*, **30**(2), 145–150.

Niandou, H., Shao, J.-F., Henry, J.-P. and Fourmaintraux, D. (1997) Laboratory investigation of the mechanical behaviour of Tournemire shale, *Int. J. Rock Mech. Min. Sci.*, **34**(1), 3–16.

Rejeb, A. (1999) Mechanical characterization of the argillaceous Tournemire site (France), In: *Proceedings de ROCKSITE-99*, Bangalore (India), pp. 45–50.

Thouvenin, G. (1999) Modélisations couplées thermo-hydro-mécaniques en milieux poreux partiellement saturés: solutions linéaires et non linéaires, *Ph. D. thesis*, Institut Polytechnique de Lorraine, France.

Thury, M. and Bossart, P. (1999) The Mont Terri rock laboratory, a new international research project in a Mesozoic shale formation, in Switzerland, *Engineering Geology*, **52**, 347–359.